

Tokujiro Yamamoto*, Kouichi Hayashi, Naohisa Happo, and Shinya Hosokawa

X-ray Fluorescence Holography for a Ti–Nb Binary Alloy Consisting of the Martensite, Austenite and Omega Phase

DOI 10.1515/zpch-2015-0670

Received July 30, 2015; accepted December 13, 2015

Abstract: The local atomic structure near an Nb atom in a Ti–20 at.%Nb alloy single crystal, which consists of the β , α'' and ω Ti phases, was investigated by means of X-ray fluorescence holography (XFH). The atomic images were reconstructed in the vicinity of an Nb atom, which is one of the typical β stabilizing elements in β Ti alloys. Most atoms in the β Ti primary phase were reconstructed clearly. The atoms in the α'' Ti martensite phase could not be reconstructed, because the α'' Ti martensite has the crystal structure with low symmetry. Some atoms in the ω Ti fine precipitates were reconstructed successfully, although the amount of the ω Ti phase was much smaller than that of the β phase. An Nb atom and its first nearest neighbors tend to keep the BCC structure even upon the ω Ti phase formation.

Keywords: Ti Alloys, Omega Phase, Martensite, X-ray Fluorescence Holography.

1 Introduction

The β Ti alloys with a body centered cubic (BCC) structure have been one of promising materials for glass frames, surgical tools and artificial bones for re-

*Corresponding author: Tokujiro Yamamoto, Department of Mechanical and Intelligent Engineering, Utsunomiya University, 7-1-2 Yoto, 321-8585 Utsunomiya, Japan, e-mail: toku@cc.utsunomiya-u.ac.jp

Kouichi Hayashi: Department of Materials Science and Engineering, Nagoya Institute of Technology, 466-8555 Nagoya, Japan

Naohisa Happo: Department of Frontier Sciences, Graduate School of Information Sciences, Hiroshima City University, 731-3194 Hiroshima, Japan

Shinya Hosokawa: Department of Physics, Graduate School of Science and Technology, Kumamoto University, 860-8555 Kumamoto, Japan

placement, because they possess light weight, high strength, low Young's modulus and biocompatibility. The crystal structure of the α'' Ti martensite, which is formed without diffusion upon rapidly cooling from the β Ti phase, is orthorhombic with Cmc_m space group [1]. This α'' Ti martensite is also formed by applying stress. Some β Ti alloys exhibit superelastic behavior, accompanying stress-induced martensitic phase transformation from the β Ti BCC austenite phase to the α'' Ti martensite phase [2–12].

The pure Ti has the hexagonal closed-packed (HCP) structure (α Ti phase) up to 1155 K, and the β BCC Ti phase is stable from 1155 K to 1943 K. To stabilize β Ti alloys at room temperature, a certain amount Mo, Nb, Ta, W and etc., so called β stabilizing elements or β stabilizers, should be added to pure Ti. It is believed that β stabilizing elements randomly dissolve in the β Ti phase [13].

By addition of β stabilizing elements, β - α transformation temperature decreases. However, it is not enough to stabilize the β Ti phase at room temperature. To do so, high density of the fine ω Ti phase is required to be precipitated by aging heat treatment. It is considered that high density of the fine ω phase suppresses the martensitic phase transformation from the β austenite to the α'' martensite.

Formation of the ω Ti phase, having the AlB₂-type structure with P6/mmm space group, also does not accompany diffusion, similar to martensitic phase transformation [13–15]. Figure 1(a) shows the crystal structure of the β Ti BCC phase, whose lattice parameter is about 0.3 nm. Figure 1(b) schematically shows the crystal structure of the β Ti BCC phase along $\langle 1\bar{1}0 \rangle$ orientation of the β Ti phase. In Figure 1, the $\{111\}$ plane of the β Ti phase is horizontal. Hereafter, $\langle uvw \rangle$ orientation and $\{hkl\}$ plane of the β Ti phase are referred to as $\langle uvw \rangle_\beta$ and $\{hkl\}_\beta$, respectively. The BCC structure consists of the stacking sequence of three types of the $\{111\}_\beta$ planes, the planes A, B and C. Upon ω phase formation, the planes B and C displaced for $\frac{1}{12}\langle 111 \rangle_\beta$, as shown in Figure 1(c). Thus, the $\langle 111 \rangle_\beta$ and $\langle 11\bar{2} \rangle_\beta$ are parallel to $\langle 0001 \rangle_\omega$ and $\langle 1\bar{2}10 \rangle_\omega$, respectively. And the relationships between the lattice parameters of the β and ω Ti phases are $a_\omega = \sqrt{2}a_\beta$ and $c_\omega = \frac{\sqrt{3}}{2}a_\beta$, where a_β is the lattice constant of the β Ti phase.

The β Ti phase is actually stabilized at room temperature by the formation of the ω Ti phase. However, the precipitation of the ω Ti phase degrades mechanical properties of the β Ti alloys. Therefore, it is important to control the amount of the ω phase in the β Ti alloys to maintain the high strength and superelastic properties. Since the amount of the β Ti phase depends on the content of β stabilizing elements, the role of β stabilizing elements must be one of the keys to produce practical and economical β Ti alloys. In this study, we demonstrated results of X-ray fluorescence holography (XFH) [16–18] for a Ti–Nb binary alloy to clarify

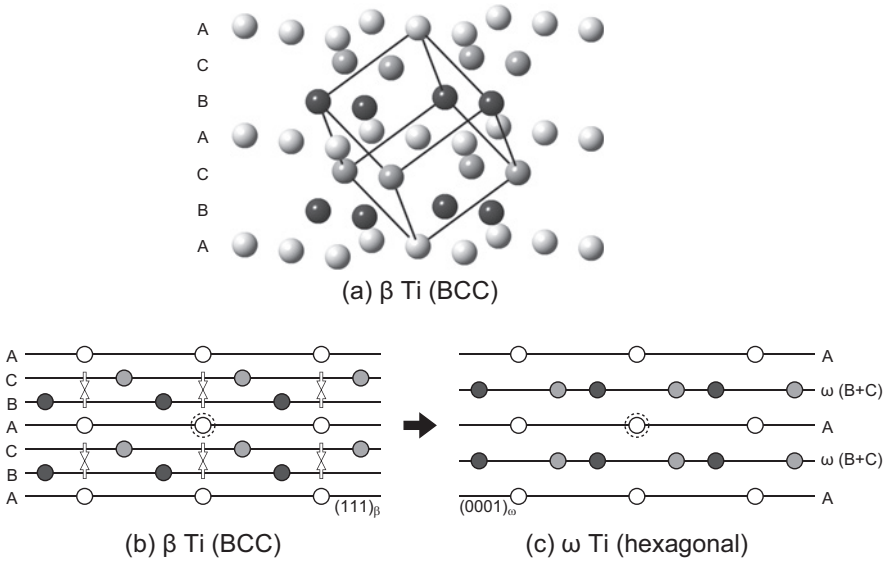


Figure 1: (a) The crystal structure of the β Ti BCC phase. The solid lines indicate the unit cell. (b) The β Ti BCC phase and (c) the ω Ti phase viewed along $\langle 1\bar{1}0 \rangle_\beta$. White arrows indicate the displacements of the $\{111\}_\beta$ upon the formation of the ω Ti phase. In this study, it is supposed that the atom surrounded by the dotted circle is an Nb atom emitting Nb–K α fluorescent X-rays.

the local atomic arrangement near an Nb atom, because the Ti–20 at.%Nb alloy is one of the prototype β Ti alloys exhibiting superelastic behavior.

2 Experimental procedures

Ti–20 at.%Nb binary alloy ingots were prepared by using arc-melting in an Ar atmosphere. At the beginning of arc-melting of Ti and Nb pieces, only Nb pieces were melted first and followed by melting Ti, because the melting point of Nb is much higher than that of Ti. The alloyed ingots of Ti and Nb were arc-melted repeatedly to make the ingots homogeneous. Finally, the Ti–Nb binary alloy ingots were melted into two rods. By using the two rods, a Ti–Nb single crystal was grown by means of a floating zone melting technique. The grown crystal was sliced into disks whose dimension was about 2 mm in thickness and 8 mm in diameter. Some disk specimens were subjected to heat treatment at 1123 K for 2 h for homogenization in an Ar atmosphere, and followed by water-quenching.

Then, the sliced specimens were subjected to heat treatment at 573 K for 0.5 h to form the ω Ti phase by aging, also followed by water-quenching.

The microstructures of one of the heat-treated sliced specimens of the single crystal were examined by using a transmission electron microscope (TEM) operated at an acceleration voltage of 200 kV. The foil specimens for TEM observation were prepared by Ar ion-milling at room temperature.

Nine X-ray fluorescence holograms were recorded by collecting Nb- $K\alpha$ X-rays, which was excited by incident X-rays at 19.5 to 23.5 keV at the beamline BL39XU in SPring-8. The holograms were symmetrized according to the structure of the β Ti BCC phase.

3 Results and discussion

Figure 2 shows the TEM microstructures of the heat-treated sliced single crystal specimen. The primary phase in the single crystal was the β Ti BCC austenite, as shown in Figure 2(a). The β Ti BCC austenite phase contains a high density of the fine ω Ti precipitates, which are bright fine domains in the dark-field image in Figure 2(b). The dimension of the ω Ti precipitates was about 5–15 nm. However, the orthorhombic martensite was often found with high density of the fine ω Ti precipitates (Figure 2(c)). In the martensite phase, martensite twins formed by self-accommodation were observed. Thus, the Ti–Nb single crystal consists of the β Ti BCC austenite with a high density of the fine ω Ti precipitates and the α'' orthorhombic martensite.

Figure 3 shows one of the normalized X-ray fluorescence holograms recorded for the Ti–Nb single crystal and used in this study. The hologram is viewed along $\langle 111 \rangle_{\beta}$. The hologram was summed according to the four-fold rotational symmetry around the $\langle 100 \rangle_{\beta}$ axis and the mirror symmetry to the $\{100\}_{\beta}$ plane. Because the primary phase is the β Ti BCC austenite, the hologram exhibits six-fold rotational symmetry around the $\langle 111 \rangle_{\beta}$ axis.

Figure 4 shows the reconstructed atomic images near an Nb atom emitting Nb- $K\alpha$ fluorescent X-rays in the $\{111\}_{\beta}$ plane as a function of z , which is the distance from the plane including the Nb emitter. The planes A, B, C and ω indicate the $\{111\}_{\beta}$ atomic planes depicted in Figure 1. The Nb atom is located at the center of the plane A at $z = 0.00 \text{ \AA}$. The plane A belongs to both the β and ω phases, the planes B and C belong to the β Ti BCC austenite, and the plane ω belongs to the ω Ti phase. The circles drawn by dotted lines indicate the ideal atomic positions for the β and ω Ti phases. The ideal atomic positions in the planes A, B and C of the β Ti phase are marked by the green, red and blue circles, respectively. The ideal

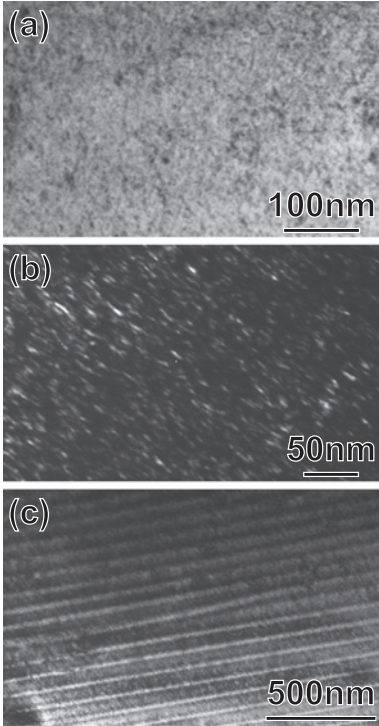


Figure 2: (a) Bright and (b) dark field TEM images of the β Ti BCC austenite with high density of the ω Ti phase. (c) The α'' Ti martensite phase was also often observed. The dark matrix and the bright fine precipitates in (b) are the β and ω phases, respectively.

atomic positions in the plane ω are also marked by the red and blue circles, since the plane ω is composed of the displaced planes B and C.

Because the primary phase is the β Ti BCC phase, most of the atomic images of the β Ti phase are reconstructed at the ideal atomic positions in the planes A, B and C. As shown in Figure 1, the planes A do not move upon formation of the ω Ti phase. Therefore, it is expected that the atoms in the planes A are reconstructed more clearly than the planes B, C and ω . However, the intensity of the three atoms, one of them is marked by q , in the plane B at $z = 1.06 \text{ \AA}$ is the highest, because these atoms are the first nearest neighboring atoms to the Nb atom emitting the Nb–K fluorescent X-rays. The three central atoms, one of them is marked by r , in the plane C at $z = 1.94 \text{ \AA}$ are hardly observed, even though the distance between the Nb atom and those three atoms are shorter than the atoms marked by r' in the plane C. Figure 5 shows the maximum intensity of the reconstructed atomic images in the 0.1 nm square at the position q in the plane B and the position r in the plane C, as a function of the distance from the plane including an Nb atom along $\{111\}_\beta$. The intensity of the reconstructed atomic images near the q position is considerably low not only in the plane C but also near the plane C.

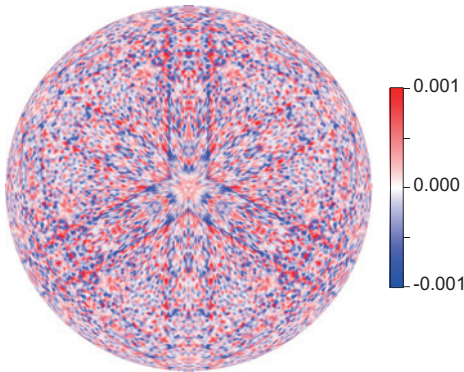


Figure 3: Normalized X-ray fluorescence hologram recorded by using Nb–K α fluorescent X-rays excited at 23.0 keV viewed along $\langle 111 \rangle_{\beta}$.

For the ω and α'' Ti phases, only some atoms could be reconstructed. Although the symmetry of the ω Ti phase is different from that of the β Ti phase, some atomic images in the plane ω at $z = 1.38 \text{ \AA}$ were reconstructed. The atomic images in the three red circles in the center of the plane ω in Figure 4 are successfully reconstructed, while those in the three blue circles in the center of the same plane are hardly observed. The atoms in the α'' orthorhombic martensite cannot be observed, because the α'' orthorhombic martensite seldom has atoms whose position is unchanged upon martensitic phase transformation.

As we have mentioned the weak atomic images in the planes C and ω for the β and ω Ti phases, some atomic images in the plane B are also weak. In the plane B at 1.06 \AA in Figure 4, the intensity of the atomic image q' is weaker than those of the atomic images q and q'' . To discuss the difference in the intensity of the reconstructed atomic images in those planes, further XFH experiments for a Ti–Nb single crystal without α'' martensite and consisting only of the β and ω Ti phases should be performed.

In this study, it is difficult to discuss on the α'' and ω Ti phases because of the low crystalline symmetry and because of the small amount of the phase, respectively. For the β Ti phase, the intensity of the reconstructed atomic images of the first nearest neighbors to an Nb atom in the plane B is remarkably high. On the contrary, the second nearest neighbors to the Nb atom do not exist at the ideal site of the BCC structure exactly. Therefore, it is considered that an Nb atom and its first nearest neighbors tend to keep the BCC structure even upon the ω Ti phase formation.

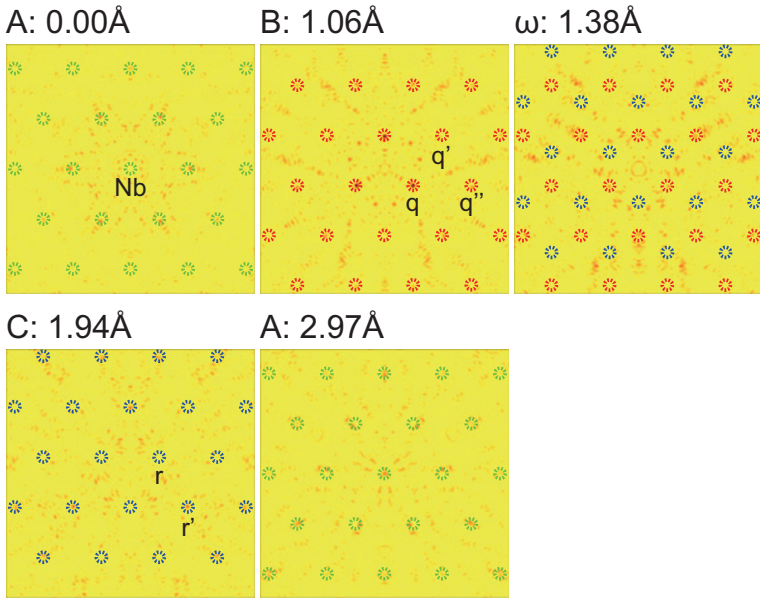


Figure 4: The atomic images near an Nb atom reconstructed from the holograms, as a function of z , the distance from the plane including an Nb atom. The distance from the $\{111\}_\beta$ plane including an Nb atom, z , is given at the upper part of each image. The side of the yellow squares is 20 Å. The green, red and blue circles drawn by dotted line indicate the ideal atomic positions for the β and ω Ti phases.

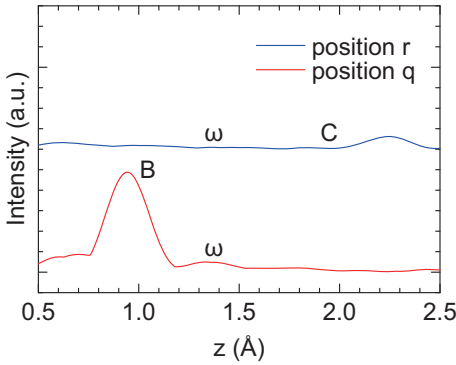


Figure 5: The intensity of the reconstructed atomic images for the positions q and r , as a function of z , the distance from the $\{111\}_\beta$ plane including an Nb atom.

4 Conclusions

The local atomic structure near a typical β stabilizing atom, Nb, in the binary β Ti alloy single crystal consisting of the β , α'' and ω phases was examined by means of XFH. Most atoms in the β Ti matrix and some in the ω Ti fine precipitates were successfully reconstructed. However, the atoms in the α'' Ti phase were not reconstructed because of low crystallographic symmetry. An Nb atom, which is one of the typical β stabilizing elements, and its first nearest neighbors tend to keep the BCC structure even upon the ω Ti phase formation.

Acknowledgement: The experiments were performed at the BL39XU beamline in the SPring-8 with the approval of the Japan Synchrotron Radiation Research Institute (Proposal No. 2010B1101). Preparation of the specimen used in this study was supported by the cooperative research of the CRDAM-IMR, Tohoku University. This work was partially supported by JSPS Grant-in-Aid for Scientific Research (B) (No. 22360264), Challenging Exploratory Research (No. 21654039) and Scientific Research on Innovative Areas “3D Active-Site Science” (No. 15H01040). This work was also supported by Cross-ministerial Strategic Innovation Promotion Program (SIP).

References

1. D. L. Moffat and D. C. Larbalestier, *Metall. Trans. A* **19** (1988) 1677.
2. H. Y. Kim, Y. Ikehara, J. I. Kim, H. Hosoda, and S. Miyazaki, *Acta Mater.* **54** (2006) 2419.
3. M. Tahara, H. Y. Kim, H. Hosoda, and S. Miyazaki, *Acta Mater.* **57** (2009) 2461.
4. Y. Al-Zain, H. Y. Kim, T. Koyano, H. Hosoda, T. H. Nam, and S. Miyazaki, *Acta Mater.* **59** (2011) 1464.
5. E. Takahashi, T. Sakurai, S. Watanabe, N. Masahashi, and S. Hanada, *Mater. Trans.* **43** (2002) 2978.
6. F. Nozoe, H. Matsunomoto, T. K. Jung, S. Watanabe, T. Saburi, and S. Hanada, *Mater. Trans.* **48** (2007) 3007.
7. T. Zhou, M. Aindow, S. P. Alpay, M. J. Blackburn, and M. H. Wu, *Scripta Mater.* **50** (2004) 343.
8. D. Kuroda, M. Niinomi, M. Morinaga, Y. Kato, and T. Yashiro, *Mat. Sci. Eng. A-Struct.* **243** (1998) 244.
9. Q. Li, M. Niinomi, M. Nakai, Z. Cui, S. Zhu, and X. Yang, *Metall. Mater. Trans. A* **42** (2011) 2843.
10. A. Biesiekierski, J. Wang, M. A. H. Gepreel, and C. Wen, *Acta Biomater.* **8** (2012) 1661.
11. H. Tada, T. Yamamoto, X. Wang, and H. Kato, *Mater. Trans.* **53** (2012) 1981.
12. H. Tada, T. Yamamoto, X. Wang, and H. Kato, *Mater. Trans.* **54** (2013) 1502.

13. B. S. Hickman, *J. Mater. Sci.* **4** (1969) 554.
14. D. de Fontaine and O. Buck, *Philos. Mag.* **27** (1973) 967.
15. T. S. Kuan and S. L. Sass, *Philos. Mag.* **36** (1977) 1473.
16. G. Faigel, M. Tegze, S. Marchesini, and M. Belakhovsky, *J. Electron Spectrosc.* **114–116** (2001) 1063.
17. K. Hayashi, *Adv. Imag. Elect. Phys.* **140** (2006) 119.
18. K. Hayashi, N. Happo, S. Hosokawa, W. Hu, and T. Matsushita, *J. Phys.-Condens. Mat.* **24** (2012) 093201.